### nature physics

**Article** 

https://doi.org/10.1038/s41567-024-02429-9

# Melting of the charge density wave by generation of pairs of topological defects in UTe,

Received: 12 June 2023

Accepted: 5 February 2024

Published online: 20 March 2024



Check for updates

Anuva Aishwarya 1, Julian May-Mann<sup>1,2</sup>, Avior Almoalem 1, Sheng Ran<sup>3,4,5</sup>, Shanta R. Saha<sup>3</sup>, Johnpierre Paglione <sup>3,6</sup>, Nicholas P. Butch <sup>3,4</sup>, Eduardo Fradkin **1**,2 & Vidya Madhavan **1**,6

Topological defects are singularities in an ordered phase that can have a profound effect on phase transitions and serve as a window into the order parameter. Examples of topological defects include dislocations in charge density waves and vortices in a superconductor or pair density wave, where the latter is a condensate of Cooper pairs with finite momentum. Here we demonstrate the role of topological defects in the magnetic-field-induced disappearance of a charge density wave in the heavy-fermion superconductor UTe<sub>2</sub>. We reveal pairs of topological defects of the charge density wave with positive and negative phase winding. The pairs are directly correlated with zeros in the charge density wave amplitude and increase in number with increasing magnetic field. A magnetic field generates vortices of the superconducting and pair density wave orders that can create topological defects in the charge density wave and induce the experimentally observed melting of this charge order at the upper critical field. Our work reveals the important role of magnetic-field-generated topological defects in the melting of the charge density wave order parameter in UTe<sub>2</sub> and provides support for the existence of a pair density wave order on the surface.

Ordered phases that break continuous symmetries, such as superconductors, magnets, liquid crystals and charge density wave (CDW) systems, can host special topological defects<sup>1-3</sup> such as vortices<sup>4,5</sup>, skyrmions  $^{6-8}$ , disclinations  $^{1-3}$  and dislocations  $^{9-11}$ . In general, although a defect is a simple phase slip in the order parameter, a topological defect is one that cannot be repaired by a continuous order parameter change. Such defects are associated with a phase winding of the order parameter in integer multiples of  $2\pi$  (Fig. 1d), with the order parameter going to zero at the defect centre. The detailed behaviour of topological defects can be used as a window into the nature of the ordered phase. A famous example is the case of superfluid <sup>3</sup>He where the sub-phases in the superfluid state can be classified by the nature of the superconducting vortices<sup>12,13</sup>. Additionally, in contrast to the usual melting of an order parameter via a continuous suppression of amplitude, the generation of topological defects can play a critical role in phase transitions. The latter occurs in the famous Berezinskii-Koster litz-Thoulesstransition<sup>14–18</sup> in two dimensions, where the long-range order of the XY model is destroyed by the thermal generation and proliferation of pairs of topological defects with opposite winding. Similarly, applying a magnetic field to a type-II superconductor leads to the creation of

Department of Physics and Materials Research Laboratory, University of Illinois at Urbana-Champaign, Urbana, IL, USA. Anthony J. Leggett Institute for Condensed Matter Theory, University of Illinois, Urbana, IL, USA. 3Maryland Quantum Materials Center, Department of Physics, University of Maryland, College Park, MD, USA. ANIST Center for Neutron Research, National Institute of Standards and Technology, Gaithersburg, MD, USA. Department of Physics, Washington University in St Louis, St Louis, MO, USA. 6Canadian Institute for Advanced Research, Toronto, ON, Canada. 🖂 e-mail: vm1@illinois.edu

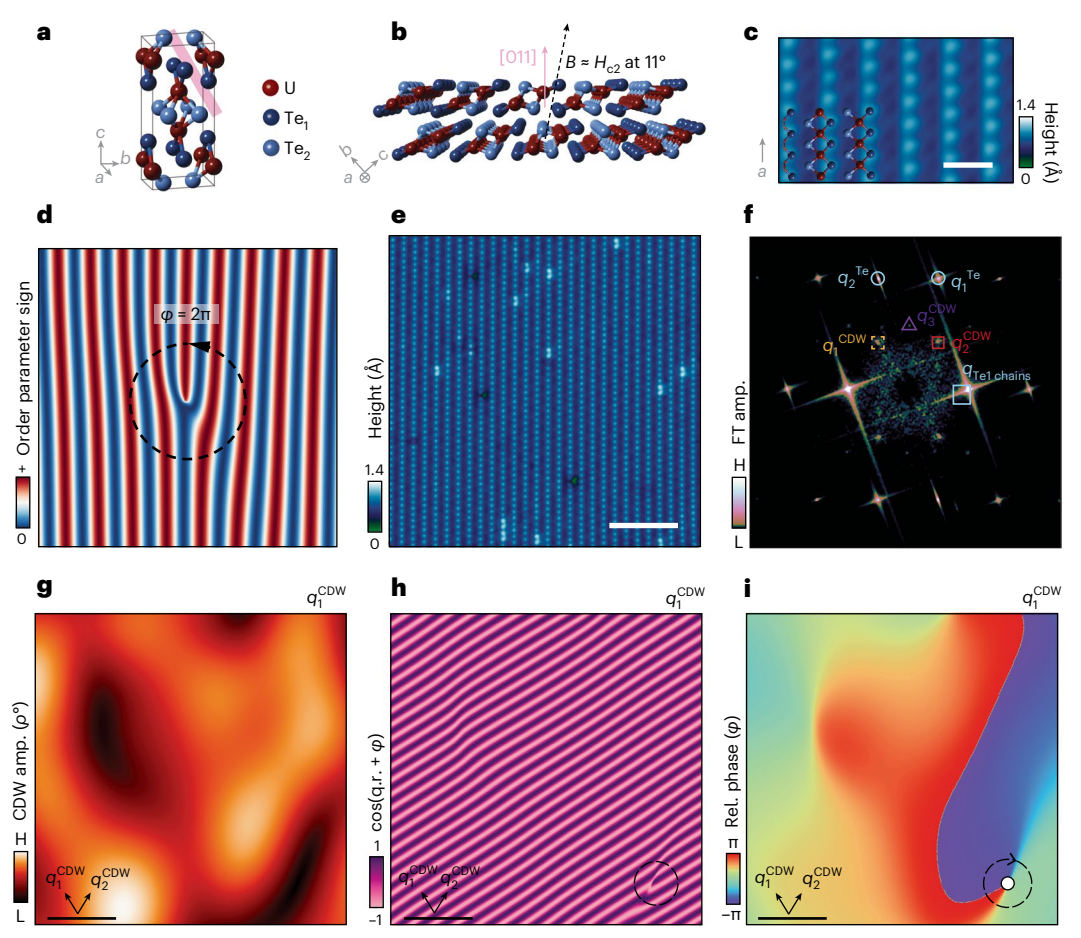


Fig. 1 | Topological defects in the CDW in UTe<sub>2</sub> and their relationship to the amplitude and phase of the CDW. a, Unit cell of UTe<sub>2</sub> with the (011) cleave plane shown by the pink rectangle. b, Schematic of the (011) direction and the relative orientation of the applied magnetic field with respect to the (011) direction used in this study. c, Atomically resolved topography of the surface of UTe<sub>2</sub>, showing the Te1 and Te2 atoms, with an overlay of the atoms of the cleave plane as a guide to the eye. Scale bar, 10 Å. d, Schematic of a dislocation or a topological defect in an ordered phase where the phase winds by  $2\pi$ . e, High-resolution topography on

the (011) surface of UTe<sub>2</sub>, showing the Te1 and Te2 atoms (V = -40 mV, I = 120 pA, T = 300 mK). Scale bar, 50 Å. **f**, FT of the topography shown in **e**, with the lattice Bragg peaks and CDW peaks marked. **g**-**i**, Amplitude (**g**),  $\cos(\mathbf{q_i}.\mathbf{r} + \phi_1(\mathbf{r}))$  (**h**) and relative phase maps (**i**) of the order parameter associated with  $\mathbf{q_i}^{\text{CDW}}$ . Scale bars, 50 Å. **h**, **i**, Position of an isolated topological defect in the CDW. The topography and various maps shown here have been cropped and aligned from a larger field of view for ease of visualization. Supplementary Figs. 2 and 3 provide the original topography and relative phase maps for both components of the CDW.

vortices, the number of which increases as the magnetic field increases, until the superconductivity is destroyed at the upper critical field  $H_{\rm c2}$  (refs. 4,5). Phase transitions through the generation of topological defects appear not only in condensed-matter physics but also in other areas of physics like studies of the early Universe<sup>19</sup>.

UTe<sub>2</sub> is a heavy-fermion superconductor that exhibits an extremely rich phase diagram with pressure, temperature and magnetic field<sup>20,21</sup> including a low-temperature, magnetic-field-sensitive charge order on its surface strongly intertwined with superconductivity<sup>22</sup>. In this work, we employ high-resolution scanning tunnelling microscopy (STM) and spectroscopic imaging to visualize the generation of pairs of topological defects with opposite phase windings that are responsible for the magnetic-field-induced melting of the unconventional CDW in UTe<sub>2</sub> (ref. 22). UTe<sub>2</sub> crystallizes into a body-centred orthorhombic structure with the space group Immm (Fig. 1a). The crystal has two types of Te atom based on the relative U-Te bond lengths (Fig. 1a). UTe<sub>2</sub> is a Kondo metal below about 30.0 K and superconducts below 1.6 K (Supplementary Fig. 1a shows the transport characterization). UTe<sub>2</sub> single crystals used in this study were cleaved at ~90 K in an ultrahigh vacuum and immediately inserted into the STM head. The (011) plane of the crystal is the easy-cleave plane, and cleaving along this plane exposes chains of Te1 and Te2 atoms that align along the crystallographic a direction (Fig. 1b). Figure 1c shows atomically resolved STM topography with the schematic of the atomic sites overlaid. Figure 1e shows the large-area atomically resolved STM topography obtained at 300 mK. Figure 1f shows the Fourier transform (FT) corresponding to the topography shown in Fig. 1e, where the Bragg peaks corresponding to the Telattice  $(\mathbf{q}_{12}^{\text{Te}})$  and the additional modulations corresponding to incommensurate CDWs ( $\mathbf{q}_{1,2,3}^{\text{CDW}}$ ) are labelled <sup>22</sup>. The CDW order parameter has an amplitude and phase, both of which can vary as a function of position in real space. The three incommensurate CDW orders in UTe<sub>2</sub> can be mathematically expressed as  $\rho_{q_i}(\mathbf{r}) = \rho_{q_i}^o(\mathbf{r}) \cos(\mathbf{q_i}.\mathbf{r} + \phi_i(\mathbf{r})), i = 1, 2, 3$ , where  $\rho_a^o(\mathbf{r})$  is the amplitude of the *i*th CDW and  $\cos(\mathbf{q_i} \cdot \mathbf{r} + \phi_i(\mathbf{r}))$  captures the periodic modulation of the CDW. We refer to  $\phi_i(\mathbf{r})$  as the relative phase of the CDW to distinguish it from  $\mathbf{q_i}$ . The relative phase of the CDW can vary in real space (due to dislocations, for example). Our goal in this work is to use the information contained in the amplitude  $ho_{q_i}^o(\mathbf{r})$  and relative phase  $\phi_i(\mathbf{r})$  to determine the mechanism of the magnetic-field-induced melting of CDWs in UTe2.

The technique to determine the spatial variations in the amplitude and relative phase of each CDW is as follows. We first perform inverse Fourier filtering of the CDW peaks in the FT to isolate the signal associated with the CDW modulation. To visualize the amplitude and modulating component for the CDW in real space, we take the modulus and cosine of the argument of this signal and plot those as a function of position **r**. Supplementary Information provides more details of this

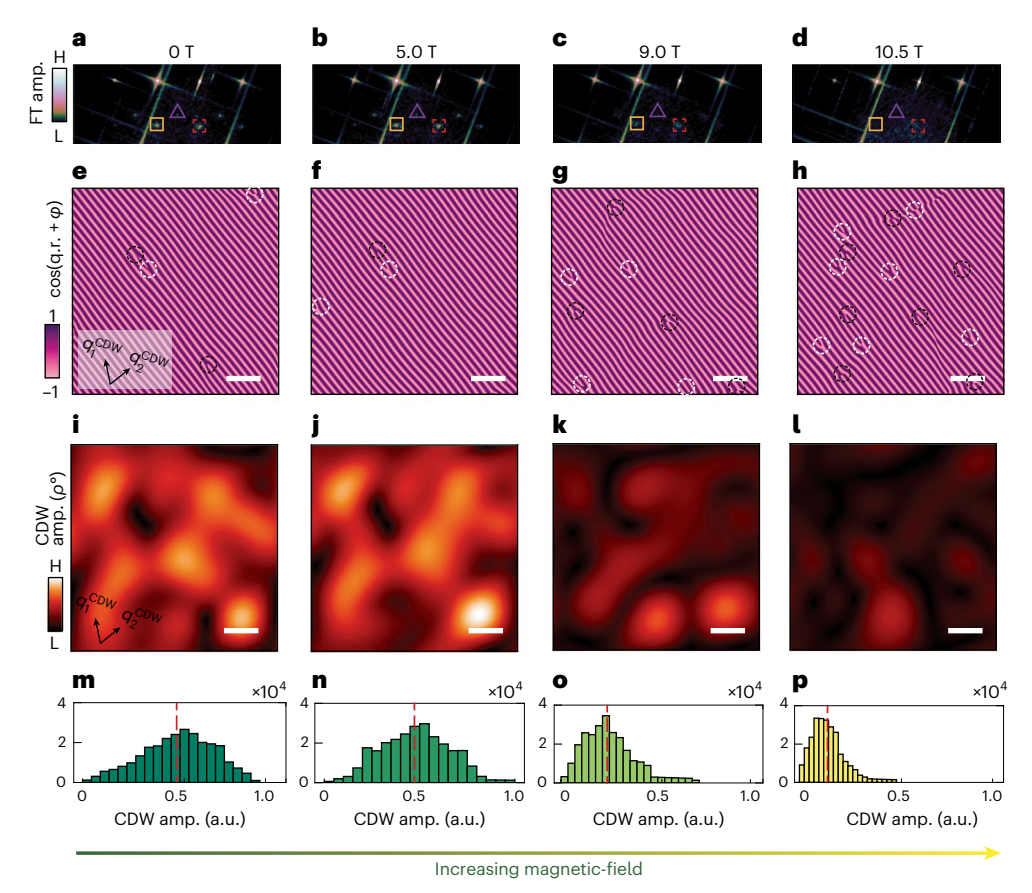


**Fig. 2** | **Generation of topological defects in the phase of CDW and decay of the amplitude with increasing magnetic field. a–d,** FT of topographies obtained on the same area as a function of increasing magnetic field at T = 300 mK. The CDW peaks are marked by squares and triangle. The  $\mathbf{q}_2$  CDW peak used to obtain the maps of amplitude and modulating part is shown by the dashed square.  $\mathbf{e}$ – $\mathbf{h}$ ,  $\cos(\mathbf{q}_2.\mathbf{r}+\phi_2(\mathbf{r}))$  maps of  $\mathbf{q}_2$  CDW as a function increasing magnetic field, showing an increasing number of dislocations and anti-dislocations (indicated by

black and white dashed circles, respectively). The CDW directions have been marked in  ${\bf e}$  as a reference.  ${\bf i}$ – ${\bf l}$ , Suppression of amplitude shown by amplitude maps of  ${\bf q}_2^{\rm CDW}$  as a function of increasing magnetic field in the same field of view. The CDW directions have been marked in  ${\bf i}$  as a reference.  ${\bf m}$ – ${\bf p}$ , Histogram of the amplitude maps of  ${\bf q}_2^{\rm CDW}$  as a function of increasing magnetic field, where the mean amplitude is indicated by the red dashed line. Scale bars, 50 Å.

process. To illustrate the types of dataset and information contained in them, we use this technique to obtain the three quantities  $\rho_{q_1}^o(\mathbf{r})$ ,  $\cos(\mathbf{q_1}.\mathbf{r}+\phi_1(\mathbf{r}))$  and  $\phi_1(\mathbf{r})$  for  $\mathbf{q_1}^{\text{CDW}}$  (labelled in the FT data in Fig. 1f). The resulting images are shown in Fig. 1g–i. Supplementary Fig. 3 shows a similar analysis performed for  $\mathbf{q_2}^{\text{CDW}}$ . At zero magnetic field, we observe very few dislocations of the CDW consistent with long-range CDW order. However, some regions have dislocations as those shown in Fig. 1h (Supplementary Figs. 3 and 4). The dislocations are topological defects in the CDW order and can be seen as a phase winding in the relative phase  $(\phi_1(\mathbf{r}))$  map shown in Fig. 1i (Supplementary Figs. 3 and 4).

Prior work has shown that the CDW order parameter is suppressed with the magnetic field and disappears close to  $H_{\rm c2}$  (ref. 22), and our goal is to determine the role of topological defects in this phase transition. Figure 2a–d shows a series of FTs of topographies with increasing field. As shown previously, the CDW peaks in the FTs are suppressed and eventually disappear close to  $H_{\rm c2}$ . We first look at the evolution of the modulating component of  ${\bf q_2}^{\rm CDW}$ . As the magnetic field increases, we find an increasing number of topological defects (Fig. 2e–h, circles). This holds true for  ${\bf q_1}^{\rm CDW}$  and  ${\bf q_3}^{\rm CDW}$ , too (Supplementary Figs. 5e–h and 6e–h). The primary conclusion from these maps is that an increasing magnetic field leads to an increase in the number of dislocations in all the components of the CDW. However, the positions of the dislocations in  $\rho_{q_1}^o({\bf r})$ ,  $\rho_{q_2}^o({\bf r})$  and  $\rho_{q_3}^o({\bf r})$  are not necessarily the same, which is discussed later.

We now turn our attention to the amplitude maps that show a steady decrease in the overall amplitude for all the components of CDW as function of the field (Fig. 2i–l, where all the plots have the same intensity scale; Supplementary Figs. 5a–d and 6a–d show the data for  ${\bf q}_2^{CDW}$  and  ${\bf q}_3^{CDW}$ , respectively). This is clearly reflected in the histograms of the amplitude values (Fig. 2m–p), which show that the mean value of the distribution (indicated by the red dashed line) decreases with an increasing field.

The natural next question is whether the amplitude suppression with magnetic field is caused by the increasing number of topological defects, or if they are independent. In fact, the CDW amplitude necessarily goes to zero at the centre of the topological defect. Could the generation of these topological defects be the mechanism by which the CDW is destroyed? To answer this question, we create a 'zero-amplitude' map, that is, a map of areas where the amplitude is within a small range of zero (Fig. 3a,b), and compare this with a map of the locations of topological defects in same field of view (Fig. 3c,d). The 'zero-amplitude' map was created with a binary mask for the zero-amplitude region using 5% thresholding. Comparing Fig. 3b,d, we find that the zero-amplitude areas and the sites of topological defects have a direct one-to-one correspondence. This is borne out by the strong positive cross-correlation between the two maps (value of 0.6, where +1/-1 indicates very strong positive/negative correlation (Fig. 3e)). A similar analysis performed for  $\mathbf{q}_1^{\text{CDW}}$  shows a cross-correlation value of 0.7 (Supplementary Fig. 7). Our data indicate that the amplitude  $\rho_{a}^{o}$  does not uniformly diminish in real space. Instead, the magnetic field generates topological defects that punch holes in the amplitude field. These data provide compelling evidence for the magnetic-field-induced melting of the CDW order

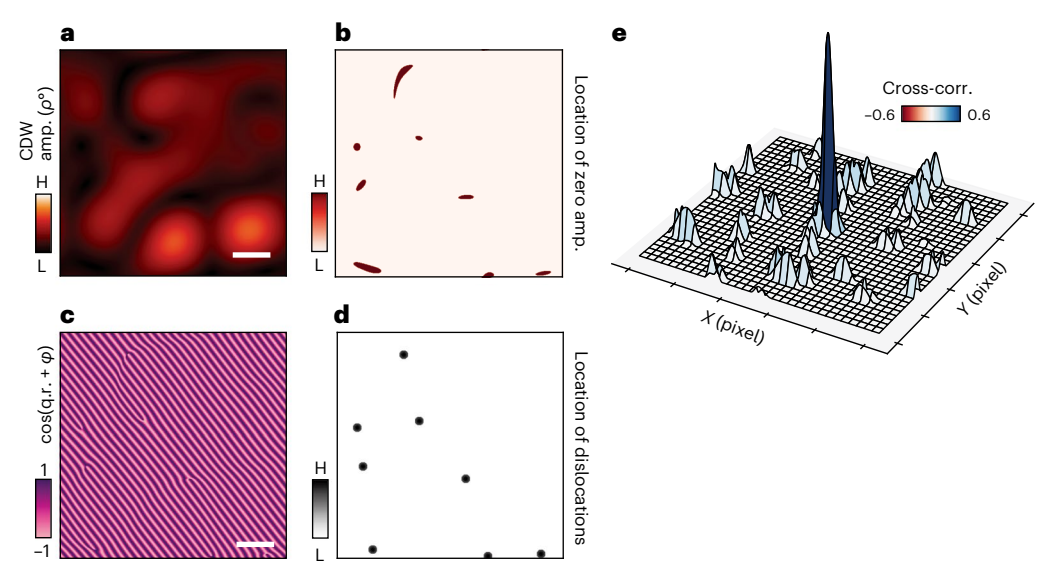


Fig. 3 | Strong positive cross-correlation between regions of zero-amplitude and location of topological defects. a, Amplitude map of  $\mathbf{q}_2$ CDW obtained at B=9 T, T=300 mK. b, Zero-amplitude mask generated by 5% thresholding from the amplitude map that shows regions of zero amplitude. Scale bars, 50 Å. c,  $\cos(\mathbf{q}_2.\mathbf{r}+\phi_2(\mathbf{r}))$  map of  $\mathbf{q}_2$ CDW on the same field of view as a. d, Binary mask

of the position of dislocations obtained from  $\mathbf{c}$ . Each dislocation is represented by a circular Gaussian function.  $\mathbf{e}$ , Two-dimensional cross-correlation of the normalized masks shown in  $\mathbf{b}$  and  $\mathbf{d}$  with a value 0.6 at the centre, indicative of a positive cross-correlation. A similar cross-correlation value is obtained on analysing  $\mathbf{q}_1^{CDW}$  (Supplementary Fig. 7).

parameter in  $UTe_2$  through the generation of an increasing number of topological defects.

The description above bears marked resemblance to the vortex state of a type-II superconductor where the superconducting order parameter goes to zero inside vortex cores, whereas still being finite outside it. Vortices are topological defects where the phase of the order parameter winds by multiples of  $2\pi$ , and can occur in any ordered phase. To visualize this phase winding around a CDW dislocation, we plot the relative phase as a function of angle for two different dislocations (Fig. 4). We find that in a non-zero magnetic field, the CDW hosts both dislocations and anti-dislocations with opposite vorticities (where the relative phase winds by  $+2\pi$  and  $-2\pi$ , as shown in Fig. 4e,f, respectively). A polar plot far away from the dislocation shows a constant relative phase, as expected (Fig. 4g). Both dislocations and anti-dislocations are expected since there is no preferred orientation for Burger's vectors (provided they are parallel to the CDW wavevector). This is unlike superconducting vortices generated by a magnetic field, which have a preferred winding set by the direction of the magnetic field. Interestingly, an examination of the phase maps with an increasing magnetic field shows that the defects occur in dislocation-anti-dislocation pairs (indicated by pairs of black and white circles in Fig. 4e-g), which prefer to remain close to each other. This makes energetic sense, as net vorticity costs extra energy, and dislocations of opposite vorticity can minimize energy by pairing up.

Previous work  $^{22}$  has suggested that this unconventional CDW in UTe $_2$  is strongly intertwined  $^{23}$  with a pair density wave (PDW) and uniform superconductivity. Additionally, Josephson STM measurements have provided evidence for a PDW with same wavevectors as the CDWs on the surface in UTe $_2$  (ref. 24), which is also confirmed by our spectroscopic measurements (Supplementary Fig. 8). A PDW state is an exotic phase of matter, a Larkin–Ovchinnikov-like state  $^{25,26}$  with finite-momentum Cooper pairs. To further understand the connection between the three aforementioned orders and the mechanism behind the magnetic-field-induced dislocations, we consider the Ginzburg–Landau free energy for a system with coexisting uniform triplet superconductivity and triplet PDWs. As previously established, this combination of superconducting orders leads to a daughter CDW order, with the same wavevector as the PDW. Here we also show that

half-vortices of the PDW (elementary defects of the PDW where the phase of  $\Delta_{+q_i}$  winds by  $2\pi$  or the phase of  $\Delta_{-q_i}$  winds by  $2\pi$ , but not both<sup>27</sup>) can also lead to dislocations and anti-dislocations in the CDW<sup>28</sup>.

We first show that half-vortices of the PDW can induce dislocations of the CDWs within the Ginzburg–Landau theory. Here we will rewrite the real CDW order parameter  $\rho_{q_i}$  as two complex components with opposite momenta, namely,  $\rho_{q_i}=\rho_{+q_i}\mathrm{e}^{\mathrm{i}\mathbf{q}_i.\mathbf{r}}+\rho_{-q_i}\mathrm{e}^{-\mathrm{i}\mathbf{q}_i.\mathbf{r}}$ , where  $\rho_{-q_i}=\rho_{+q_i}^*$ . Within this theory, there is a trilinear coupling term linking the three order parameters ( $\rho_{+q_i}$ ,  $\Delta_{\pm q_i}$  and  $\Delta_0$ ). The Landau theory equations of motion for the CDW order parameter  $\rho_{+q_i}$  are

$$\rho_{+q_i} \propto \mathbf{\Delta}_0.\mathbf{\Delta}_{-q_i}^* + \mathbf{\Delta}_0^*.\mathbf{\Delta}_{+q_i}. \tag{1}$$

The equations of motion for  $\rho_{-q_i}$  are found by complex conjugation. Dislocations and anti-dislocations are encoded as phase windings of  $\rho_{+q_i}$ . As we shall now show, a half-vortex of  $\Delta_{+q_i}$  can lead to a dislocation of  $\rho_{+q_i}$  (positive phase winding) and a half-vortex of  $\Delta_{-q_i}$  can lead to an anti-dislocation of  $\rho_{+q_i}$  (negative phase winding). Let us first consider a half-vortex of  $\Delta_{+q_i}$ , where  $\Delta_{+q_i} \propto \mathrm{e}^{\mathrm{i}\theta_v}$ ,  $\theta_v$  winds by  $2\pi$  around the core of the half-vortex and  $\Delta_0$  and  $\Delta_{-q_i}$  are constant. If  $|\Delta_0^*.\Delta_{+q_i}| > |\Delta_0.\Delta_{-q_i}^*|$  away from the half-vortex core, the half-vortex of  $\Delta_{+q_i}$  will lead to a dislocation of  $\rho_{+q_i}$ . However, if  $|\Delta_0^*.\Delta_{+q_i}| < |\Delta_0.\Delta_{-q_i}^*|$ , there will not be a dislocation. Similar reasoning indicates that a half-vortex of  $\Delta_{-q_i}$  will lead to an anti-dislocation of  $\rho_{+q_i}$ , if  $|\Delta_0.\Delta_{-q_i}^*| > |\Delta_0^*.\Delta_{q_i}|$  away from the half-vortex core. It is also possible that a vortex of the uniform superconducting order parameter  $\Delta_0$  can produce dislocations or anti-dislocations, but this is not expected, as discussed in the Supplementary Information.

Let us now consider the effect of an external magnetic field. Since both  $\Delta_0$  or  $\Delta_{\pm q_i}$  are charge 2e order parameters, a magnetic field will induce vortices of  $\Delta_0$  and half-vortices of  $\Delta_{\pm q_i}$ . Two PDW half-vortices must also accompany each vortex of the uniform component due to the phase locking that arises from the quartic terms proportional to  $\Delta_0.\Delta_0\Delta^*_{+q_i}.\Delta^*_{-q_i}$  and  $\Delta_0.\Delta^*_{+q_i}.\Delta_0.\Delta^*_{-q_i}$  in the Ginzburg–Landautheory. If the cores of the vortex and accompanying half-vortices occupy the same location, they will not induce any dislocations since the phase windings on the right-hand side of equation (1) cancel. However, if the

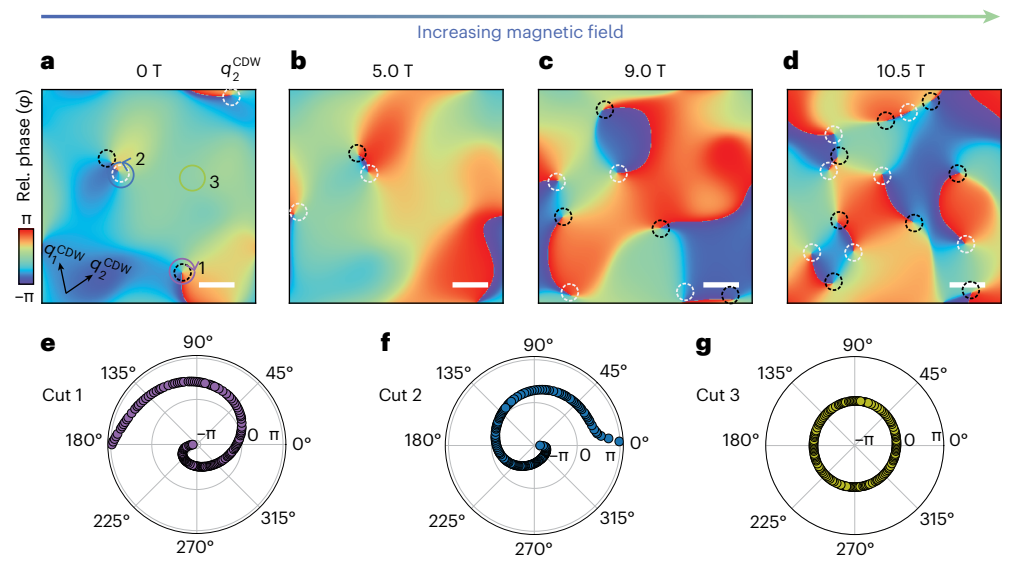


Fig. 4 | Increase in pairs of dislocations of the CDW with opposite vorticities as a function of increasing magnetic field.  $\mathbf{a}$ - $\mathbf{d}$ , Relative phase  $(\phi_2(\mathbf{r}))$  maps of  $\mathbf{q}_2^{\text{CDW}}$  as a function of magnetic field, showing increasing numbers of pairs of dislocations with opposite windings (indicated by black and white dashed circles, respectively).  $\mathbf{e}$ - $\mathbf{g}$ , Polar plots around a dislocation ( $\mathbf{e}$ ), anti-dislocation ( $\mathbf{f}$ ) and

dislocation-free (**g**) area (indicated by 1, 2 and 3, respectively, in **a**), showing the phase winding of the CDW order parameter as a function of angle. The dislocation and anti-dislocation (1 and 2) have opposite windings of the phase, whereas the phase is constant for 3. The phase winds by  $\pm 2\pi$  for 1 and 2. The plots have been obtained at the same, fixed radius from the defects.

vortex and half-vortex cores occur at different locations (that is, if all the vortices and half-vortices repel each other), then there will be local regions where there is only a single half-vortex. On the basis of our previous arguments, such isolated half-vortices may induce dislocations and anti-dislocations of  $\rho_{q_i}$  since the half-vortices of different PDW components repel each other and they can occur at different locations. This would cause the dislocations of different CDW components to occur at different locations, consistent with our data. The number of these half-vortices will increase as the magnetic field increases, which, in turn, increases the number of dislocations in the CDW. This eventually leads to the full destruction of the CDW. We can estimate the number of vortices in our field of view for a 900 nm<sup>2</sup> area, assuming a triangular Abrikosov vortex lattice for a type-II superconductor (Supplementary Fig. 9 shows a schematic). The trend in the increase in the number of CDW dislocations in all the components of the CDW qualitatively agrees with the increase in the number of vortices and the aforementioned Ginzburg-Landau theory for these intertwined orders.

In summary, we show that the sensitivity of the CDW to magnetic fields in UTe<sub>2</sub> is caused by field-generated topological defects, that is, dislocations that suppress the CDW order parameter. Although the defects can generally have positive or negative phase winding, we find that they occur in pairs with opposite windings due to energetic considerations. Our analysis also provides important information on the relationship of the CDW to a coexisting PDW state. There are two kinds of PDW that may occur. In one case, the PDW is the daughter phase arising from a combination of an existing CDW state and superconductivity<sup>29</sup>. Here, even if superconductivity is destroyed with the field, the CDW will continue to survive. In the second scenario, the PDW is the parent phase, with the CDW being the daughter order<sup>23</sup>. In this case, the CDW will disappear when either the PDW or uniform SC order are destroyed. Within the PDW scenario, on the basis of the disappearance of CDW along with superconductivity, our data and theoretical analysis suggest that the PDW is the parent phase. Given the surmounting experimental evidence pointing towards an exotic superconducting state in UTe2, this observation potentially makes UTe<sub>2</sub> a promising candidate to explore the properties of a parent PDW order on its surface.

#### **Online content**

Any methods, additional references, Nature Portfolio reporting summaries, source data, extended data, supplementary information, acknowledgements, peer review information; details of author contributions and competing interests; and statements of data and code availability are available at https://doi.org/10.1038/s41567-024-02429-9.

#### References

- Mermin, N. D. The topological theory of defects in ordered media. Rev. Mod. Phys. 51, 3 (1979).
- Chaikin, P. & Lubensky, T. Principles of Condensed Matter Physics (Cambridge Univ. Press, 1995).
- 3. Nelson, D. R. *Defects and Geometry in Condensed Matter Physics* (Cambridge Univ. Press, 2002).
- Abrikosov, A. A. On the magnetic properties of superconductors of the second group. Sov. Phys. JETP 5, 1174–1182 (1957).
- Tinkham, M. Introduction to Superconductivity (Courier Corporation, 2004).
- Barrett, S. E., Dabbagh, G., Pfeiffer, L. N., West, K. W. & Tycko, R.
   Optically pumped NMR evidence for finite-size skyrmions in GaAs quantum wells near Landau level filling v=1. Phys. Rev. Lett. 74, 5112 (1995).
- Sondhi, S. L., Karlhede, A., Kivelson, S. A. & Rezayi, E. H. Skyrmions and the crossover from integer to fractional quantum Hall effect at small Zeeman energies. *Phys. Rev. B* 47, 16419 (1993).
- Nagaosa, N. & Tokura, Y. Topological properties and dynamics of magnetic skyrmions. Nat. Nanotechnol. 8, 899–911 (2013).
- 9. Lee, P. A. & Rice, T. M. Electric field depinning of charge density waves. *Phys. Rev. B* **19**, 3970 (1979).
- Fang, A. et al. Disorder-induced suppression of charge density wave order: STM study of Pd-intercalated ErTe<sub>3</sub>. Phys. Rev. B 100, 235446 (2019).
- Lin, S. Z. et al. Topological defects as relics of emergent continuous symmetry and Higgs condensation of disorder in ferroelectrics. *Nat. Phys.* 10, 970–977 (2014).
- Salomaa, M. M. & Volovik, G. E. Quantized vortices in superfluid <sup>3</sup>He. Rev. Mod. Phys. 59, 533 (1987).

- Lounasmaa, O. V. & Thuneberg, E. Vortices in rotating superfluid <sup>3</sup>He. Proc. Natl Acad. Sci. USA 96, 7760–7767 (1999).
- Kosterlitz, J. M. & Thouless, D. J. Long range order and metastability in two dimensional solids and superfluids. (Application of dislocation theory). J. Phys. C: Solid State Phys. 5, L124 (1972).
- Kosterlitz, J. M. & Thouless, D. J. Ordering, metastability and phase transitions in two-dimensional systems. *J. Phys. C: Solid State Phys.* 6, 1181–1203 (1973).
- Berezinskii, V. L. Destruction of long-range order in one-dimensional and two-dimensional systems possessing a continuous symmetry group. II. Quantum systems. Sov. Phys. JETP 34, 610 (1972).
- Halperin, B. I. & Nelson, D. R. Theory of two-dimensional melting. Phys. Rev. Lett. 41, 121–124 (1978).
- 18. Young, A. P. Melting and the vector Coulomb gas in two dimensions. *Phys. Rev. B* **19**, 1855 (1979).
- Vilenkin, A. & Shellard, E. P. S. Cosmic Strings and Other Topological Defects (Cambridge Univ. Press, 1994).
- Ran, S. et al. Nearly ferromagnetic spin-triplet superconductivity. Science 365, 684–687 (2019).
- 21. Ran, S. et al. Extreme magnetic field-boosted superconductivity. *Nat. Phys.* **15**, 1250–1254 (2019).
- Aishwarya, A. et al. Magnetic-field-sensitive charge density waves in the superconductor UTe<sub>2</sub>. Nature 618, 928–933 (2023).
- Fradkin, E., Kivelson, S. A. & Tranquada, J. M. Colloquium: theory of intertwined orders in high temperature superconductors. *Rev. Mod. Phys.* 87, 457 (2015).

- 24. Gu, Q. et al. Detection of a pair density wave state in UTe<sub>2</sub>. *Nature* **618**, 921–927 (2023).
- Larkin, A. I. & Ovchinnikov, Y. I. Inhomogeneous state of superconductors. Sov. Phys. JETP 20, 1629–1636 (1965).
- Agterberg, D. F. et al. The physics of pair-density waves: cuprate superconductors and beyond. *Annu. Rev. Condens. Matter Phys.* 11, 231–270 (2020).
- Berg, E., Fradkin, E. & Kivelson, S. A. Charge-4e superconductivity from pair-density-wave order in certain high-temperature superconductors. *Nat. Phys.* 5, 830–833 (2009).
- Agterberg, D. F. & Tsunetsugu, H. Dislocations and vortices in pair-density-wave superconductors. *Nat. Phys.* 4, 639–642 (2008).
- 29. Liu, X., Chong, Y. X., Sharma, R. & Davis, J. S. Discovery of a Cooper-pair density wave state in a transition-metal dichalcogenide. *Science* **372**, 1447–1452 (2021).

**Publisher's note** Springer Nature remains neutral with regard to jurisdictional claims in published maps and institutional affiliations.

Springer Nature or its licensor (e.g. a society or other partner) holds exclusive rights to this article under a publishing agreement with the author(s) or other rightsholder(s); author self-archiving of the accepted manuscript version of this article is solely governed by the terms of such publishing agreement and applicable law.

@ The Author(s), under exclusive licence to Springer Nature Limited 2024

#### Methods

#### STM measurements

Single crystals of UTe $_2$  were used for this measurement. The growth and characterization are mentioned in detail elsewhere $^{20}$ . Samples were cleaved in situ at -90 K and in an ultrahigh-vacuum chamber. The samples were immediately transferred to the STM head after cleaving. The STM is housed in a  $^3$ He cryostat with a base temperature of 300 mK and a superconducting magnet that can apply magnetic fields up to 11 T. The reported temperature values were measured at the  $^3$ He pot; the actual sample temperature could be slightly higher. The STM used chemically etched and annealed tungsten tips.

## Extraction of amplitude and phase maps from the topography using Fourier decomposition

STM topographies in real space  $T(\mathbf{r})$  can be thought of as a sum of various periodic signals pertaining to the atomic lattice and other modulations (for example, CDW in our case). To extract the amplitude and phase of the periodic signal, it is more convenient to shift to the Fourier space. The Fourier component of the CDW can be thought of as  $\rho_{q_i}(\mathbf{r}) = \rho_{q_i}^o(\mathbf{r})$  eignies.  $\mathbf{r} = (\mathbf{i} = 1, 2, 3)$ , where  $\rho_{q_i}^o(\mathbf{r})$  is the amplitude of the ith CDW, and  $\mathbf{q}_i^{\text{meas}}$ .  $\mathbf{r} = (\mathbf{q}_i.\mathbf{r} + \phi_i(\mathbf{r}))$ , where  $\mathbf{q}_i.\mathbf{r}$  is the perfectly modulating component of the CDW and  $\phi_i(\mathbf{r})$  captures the phase meandering due to topological defects like dislocations and discommensurations.

We first perform an inverse Fourier filtering of the CDW peaks in the FT to isolate the signal associated with the CDW modulation. This signal is  $\rho_a^o(\mathbf{r}) e^{i\mathbf{q}_i^{\text{meas.r.}}}$ . To visualize the amplitude and modulating component for CDW in real space, we take the modulus and cosine of the argument of this complex signal and plot those as a function of position. To plot the relative phase  $\phi_i(\mathbf{r})$  of the CDW signal, we multiply a modulating component  $e^{-i\mathbf{q}_i\cdot\mathbf{r}}$  to  $\rho_{q_i}(\mathbf{r})$ . Then, Phase[ $\rho_{q_i}(\mathbf{r}) e^{-i\mathbf{q}_i \cdot \mathbf{r}}$ ] = Phase[ $\rho_{q_i}^o(\mathbf{r}) e^{i\phi_i(\mathbf{r})}$ ] =  $\phi_i(\mathbf{r})$  carries the information about the phase slips in the CDW order. Therefore, we isolate the argument of  $\rho_{q_i}(\mathbf{r}) e^{-i\mathbf{q}_i \cdot \mathbf{r}}$  and plot it as a function of position  $\mathbf{r}$ . This relative phase varies between  $-\pi$  and  $\pi$ . This implies that the relative phase stays largely constant in the field of view of the topography and winds from  $-\pi$  to  $\pi$  (or vice versa) around topological defects. This process is similar to what has been described elsewhere<sup>30</sup>. To find the exact pixel coordinates of the CDW peaks in the FT, we take the centre of mass of a window of size  $\sigma = 0.17$  nm<sup>-1</sup>. We take the smallest windowing size possible that captures only the CDW signal and inverse Fourier filter the signal inside this window for the above analysis. This process is similar to the standard lock-in technique followed for the Fourier decomposition of CDWs and PDWs in cuprates<sup>31,32</sup>.

#### Data availability

The relevant data for the plots are available via the Illinois Databank at https://doi.org/10.13012/B2IDB-6515700\_V1. Source data are provided with this paper.

#### **Code availability**

Data have been obtained using Nanonis software V5 and analysed following the procedure mentioned in the Methods section using standard functions in Python 3.9.

#### References

- 30. Wang, Z. et al. Evidence for dispersing 1D Majorana channels in an iron-based superconductor. *Science* **367**, 104–108 (2020).
- Mesaros, A. et al. Topological defects coupling smectic modulations to intra-unit-cell nematicity in cuprates. Science 333, 426-430 (2011).
- Chen, W. et al. Identification of a nematic pair density wave state in Bi<sub>2</sub>Sr<sub>2</sub>CaCu<sub>2</sub>O<sub>8+x</sub>. Proc. Natl Acad. Sci. USA 119, e2206481119 (2022)

#### Acknowledgements

We thank S. Kivelson, E.-A. Kim and D. Agterberg for useful discussions. We would also like to thank I. Hayes who provided the transport characterization of the crystals during the review process. STM work at the University of Illinois, Urbana-Champaign, was supported by the US Department of Energy (DOE), Office of Science, Office of Basic Energy Sciences (BES), Materials Sciences and Engineering Division, under award no. DE-SC0022101. V.M. and J.P. acknowledge support from the Gordon and Betty Moore Foundation's EPiQS Initiative through grants GBMF4860 and GBMF9071, respectively, as well as the Canadian Institute for Advanced Research Quantum Materials Program. Theoretical work was supported in part by the US National Science Foundation through grant DMR 2225920 at the University of Illinois (E.F.). Research at the University of Maryland was supported by the Department of Energy via award no. DE-SC-0019154 (sample characterization), the National Science Foundation under grant no. DMR-2105191 (sample preparation), the Maryland Quantum Materials Center and the National Institute of Standards and Technology. S.R.S. acknowledges support from the National Institute of Standards and Technology Cooperative Agreement 70NANB17H301.

#### **Author contributions**

A. Aishwarya and V.M. conceived the experiments. The single crystals were provided by S.R., S.R.S., J.P. and N.P.B. A. Aishwarya obtained the primary STM data with help from A. Almoalem during the review process. A. Aishwarya and V.M. performed the analysis and J.M.-M. and E.F. provided theoretical input on the interpretation of the data. A. Aishwarya, V.M., J.M.-M. and E.F. wrote the paper with input from all authors.

#### **Competing interests**

The authors declare no competing interests.

#### **Additional information**

**Supplementary information** The online version contains supplementary material available at https://doi.org/10.1038/s41567-024-02429-9.

**Correspondence and requests for materials** should be addressed to Vidya Madhavan.

**Peer review information** *Nature Physics* thanks Minghu Pan, Yukio Hasegawa and the other, anonymous, reviewer(s) for their contribution to the peer review of this work.

**Reprints and permissions information** is available at www.nature.com/reprints.